Computational and Theoretical Chemistry 1191 (2020) 113026

Contents lists available at ScienceDirect

Computational and Theoretical Chemistry

journal homepage: www.elsevier.com/locate/comptc

The supramolecular host-guest complexation of Vemurafenib with β-cyclodextrin and cucurbit[7]uril as drug photoprotecting systems: A DFT/TD-DFT study

Abdulilah Dawoud Bani-Yaseen

Department of Chemistry & Earth Sciences, Faculty of Arts & Science, Qatar University, P.O. Box: 2713, Doha, Qatar

ARTICLE INFO

Keywords:
Vemurafenib
Photoprotection
Supramolecular complexes
β-cyclodextrin
Cucurbit[7]uril
DFT/TD-DFT

ABSTRACT

The supramolecular host-guest complexation of the first-line anticancer drug Vemurafenib (VFB) with β-cyclodextrin (β-CD) and cucurbit[7]uril (CB7) is computationally investigated employing the DFT/TD-DFT method in implicit aqueous solutions. The structures of the 1:1 complexes of VFB:β-CD and VFB:CB7 are stabilized by intermolecular hydrogen bonds (HB) that are oriented at the rims of the host molecules with an average length of 2.00 Å. The results of the thermodynamic quantities revealed Δ G° values of −15.3 and −6.2 kcal/mol associated with the formation of VFB:β-CD-I and VFB:CB7-I complexes, respectively. These results suggest that the supramolecular host-guest complexation of VFB with β-CD is favored over CB7, which in turn can be attributed to the formation of cooperative HBs. The stability of the examined complexes was verified as revealed by molecular dynamics analyses, where these complexes exhibited changes of only ± 0.02 kcal/mol and ± 0.06 Å in their total energy and length of key HBs, respectively.

1. Introduction

Nanotechnology has been recently considered as a central landscape for providing remedies for various complications that we face in various aspects of our lives including biomedical challenges [1–7]. One important aspect of recent nanotechnology is the development of nanocarriers for targeted drug delivery [3,6,8]. Such nanocarriers can be classified into two types based on the bonding between the drug and its nanocarriers, namely covalent and non-covalent drug carriers. Covalent bonding is widely utilized for linking the drug with its carrier [9–12]; however, the main drawbacks of this type of bonding include the retarded release of the drug at the targeted tissues and the need for multistep synthesis for producing such assemblies. On the other hand, host-guest nano-assemblies demonstrate advantageous features in this regard [13–15]. Particularly, host-guest interaction is assembled by noncovalent interactions to form facile complexes; this includes mainly hydrogen-bonding (HB), van der Waals force, π–π stacking interaction, hydrophobic/hydrophilic interaction, and electrostatic interaction [16–22]. Yet, HB is a superior noncovalent interaction that contributes significantly in stabilizing the formed complexes [17].

It is noteworthy to mention that host-guest supramolecular interactions are constructed based on the encapsulation of a guest molecule inside the nanocavity of macrocyclic molecules with specific stoichiometric ratios, where this nanostructure is stabilized by noncovalent interactions and bondings. It is important to mention that such noncovalent interaction is significantly important for probing the interaction of the substance of interest with its local molecular environments including molecular host-guest supramolecular assemblies [23–32]. Major families of macrocyclic molecules that can afford nanocavities to serve as hosts for a wide spectrum of substances include cyclodextrins (CDs) [16–20] and cucurbit[*n*]urils (CBs) [21,22]. The macromolecule is constructed from a specific number of a repeat unit (n) covalently bridged to form a geometry of hydrophobic and hydrophilic interior and exterior, respectively. Fig. 1 shows the chemical structures of two of the most common members of these two families, namely β-CD and CB7, whose structures bear six and seven repeating units, respectively. Truncated cone shape with wide and narrow rims can be noticed for CDs, whereas CBs exhibit a pumpkin shape. The main structural characteristic of these macromolecules is their hydrophobic cavities (interior) with hydrophilic exteriors that enable them to afford partial or complete encapsulation of a hydrophobic guest molecules in aqueous solutions; this includes encapsulation of pharmaceuticals. It is noteworthy mentioning that such host molecules can form inclusion complexes of specific stoichiometric ratios including 1:1 ratio. In such a ratio, one host molecule encapsulates one guest molecule to form standalone one host-guest assembly in solution.

Interestingly, such kind of structural arrangement is similar to the cell membrane, and hence its beneficial applications do not only offer to

E-mail address: abdulilah.baniyaseen@qu.edu.qa.

https://doi.org/10.1016/j.comptc.2020.113026
Received 23 July 2020; Received in revised form 29 August 2020; Accepted 6 September 2020
Available online 12 September 2020

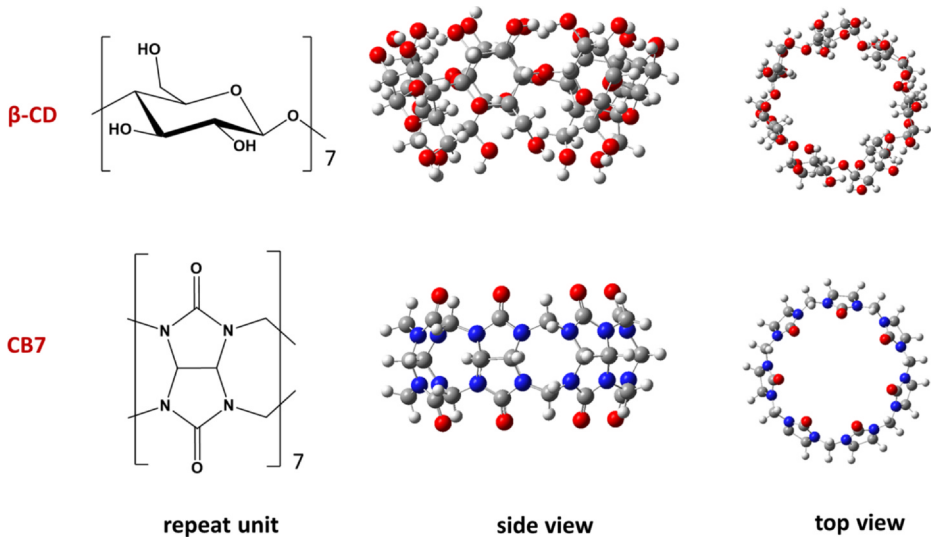

Fig. 1. Chemical structures of β-CD and CB7.

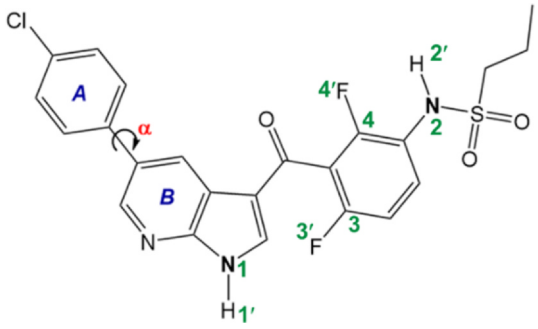

Fig. 2. Chemical structures of Vemurafenib.

enhance the pharmaceutical properties of the drugs but also examining their host-guest nanostructures is very beneficial toward providing insights into the mechanism of drug-cell membrane interaction [13–15,33–35]. Importantly, enhancing the clinical performance of pharmaceuticals has been a growing demand for promoting personalized medications worldwide. Phototoxicity is a major drawback of a wide spectrum of pharmaceuticals that are associated with exposure to light [36–39]. To this end, Vemurafenib (VFB) is a new photosensitive anticancer drug that has been recently approved by the US-FDA for the treatment of late-stage melanoma [40–43]. Using VFB b for the treatment of melanoma has demonstrated significant success [41,44]. However, the severe undesired side effects associated with the use of this photosensitive drug have become a major concern [45–47]. Thus, this necessitates elucidating the physicochemical properties and the behavior of the drug at the molecular level and accordingly provide insights concerning potential remedies for such phototoxicity. The chemical structure of VFB is shown in Fig. 2.

In this work, we study computationally the effects of the encapsulation of VFB inside the nanocavity of β-CD and CB7 molecules on its physicochemical properties. The physicochemical properties of VFB embedded in host-guest supramolecular assemblies of β-CD and CB7 in implicit aqueous solutions are examined via utilizing various approaches of the density functional theory (DFT) method. The architectures of the host-guest supramolecular assemblies and the corresponding spectral and dynamics properties are revealed at the molecular levels.

2. Computational methods

General aspects. All calculations were conducted utilizing the *Gaussian 09* (D.01) software package [48]. All calculations including geometry optimization, spectral simulation, and molecular dynamics were conducted employing the DFT method with the ωB97XD functional and 6-31 + G(d) basis set unless otherwise noted. The optimized geometries of all examined species were confirmed as a minima via conducting frequency calculations. Geometry optimization for conformational analyses of various insertion displacement inside the host's cavity was performed employing the semi-empirical method (PM7) as implemented in MOPAC-2016 software [49]. The implicit aqueous solutions were incorporated employing the integral equation formalism polarizable continuum model (IEFPCM) [50]. The absorption spectra of all examined species were simulated using the time-dependent version of the DFT method (TD-DFT). The Natural Bond Orbital analysis (NBO) and Atom Centered Density Matrix propagation (ADMP) molecular dynamics were performed as implemented in *Gaussian 09*. Optimized geometries for all species were utilized as inputs for all corresponding TD-DFT, NBO, and ADMP calculations at the same level of theory.

1:1 molecular host-guest supramolecular assemblies. The geometry of the guest and host molecules were optimized prior to forming the 1:1 molecular host-guest supramolecular assemblies. Using the corresponding optimized geometries of VFB and gusset molecules, the assemblies were constructed as illustrated in Fig. 3. The Two complexes of VFB with each of the host molecules β-CD and CB7 were constructed. For each host, the VFB molecule was included from both ends of chlorobenzene and sulfonamide units to afford two inclusion complexes I and II, respectively. The geometry optimization for each molecular host-guest supramolecular assemblies was then performed without any constrain at the same level of theory. For each of the optimized geometry of the molecular host-guest supramolecular assemblies, the dynamic stability was examined employing the ADMP molecular dynamic approach. All ADMP trajectories were constructed with a step-size of 0.2 fs for a total period of time of 60 fs.

3. Results and discussion

Considering the photochemical behavior of VFB at the molecular level, previous studies have been reported mainly on the potential photodegradation of VFB encompassing the C-F bonds [51] and affording photocaging protection for the two amine functional groups [52]. As such, we attempted herein to rationalize the effect of host-guest supramolecular inclusion complexation on the corresponding

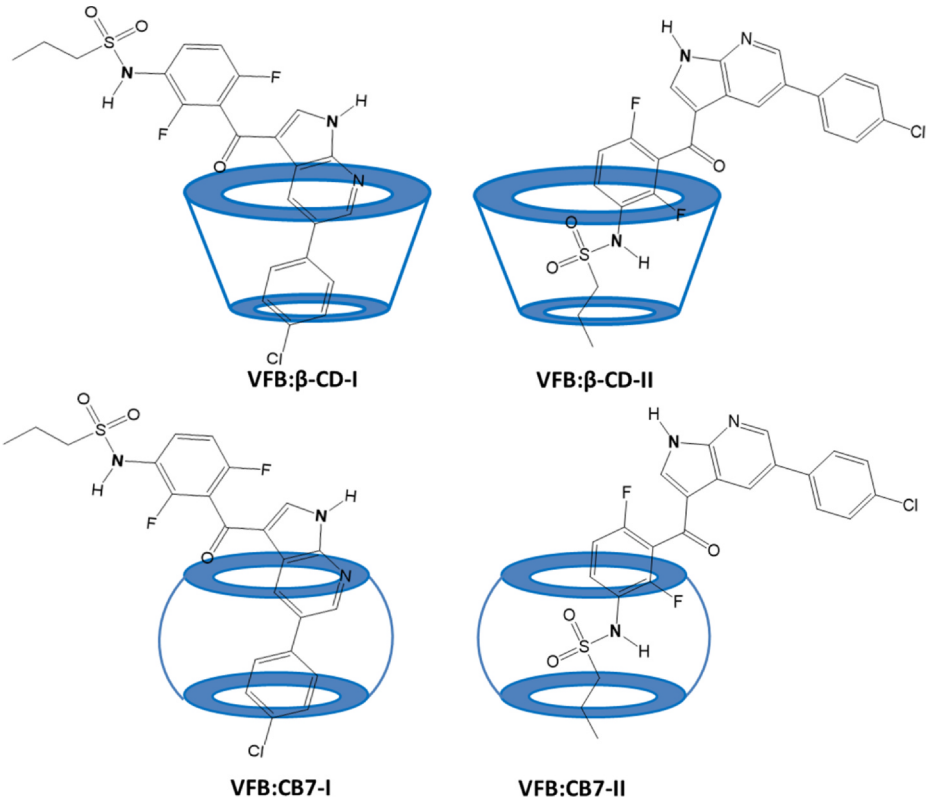

Fig. 3. Schematics of the 1:1 molecular host-guest supramolecular assemblies of VFB with β-CD and CB7.

structural properties of VFB that have a potential impact on the photochemical behavior of the drug.

Geometry optimization. The geometries of all examined species were optimized including the uncomplexed and complexed host and guest molecules employing the DFT method. The corresponding DFT calculations were performed in vacuum (gas phase) and implicit aqueous solutions. Fig. 4 shows the optimized geometries of the corresponding supramolecular host-guest inclusion complexes of VFB with β-CD and CB7 in implicit aqueous solutions obtained using the DFT/ωb97xd (6-31G(d))/IEFPCM (water) method. It is important to mention that the formation of such inclusion complexes is stabilized by noncovalent interactions including hydrogen bonding (HB). As such, we utilized herein the DFT functional of ωb97xd as it offers the best rationalization for such noncovalent interactions and the corresponding dispersion forces, and hence no attempts have been made to utilize other functionals. Interestingly, the DFT results suggest that as per the size and geometry of VFB and the examined host molecules, VFB can be partially included inside the nanocavities of both examined host molecules of β-CD and CB7. Such partial inclusions afford the opportunities for VFB to be included inside the nanocavities of the host molecules through the penetration of the chlorobenzene and sulfonamide units. Hence, as per this approach, one unit is included inside the nanocavity while the other unit remains outside the nanocavity as illustrated in Fig. 4.

As mentioned above, it is anticipated that the inclusion of VFB inside the nanocavities of the host molecule can induce structural changes on the geometry of the molecule that are attributed to noncovalent interactions. Key structural parameters of all examined species are compiled in Table 1. In accordance with the partial inclusion of VFB inside the nanocavity of the host molecule, it is worth to notice that the inclusion complexation can induce specific structural changes without affecting other properties. For example, for the length of the bonds, the DFT results revealed a N1-H1′ bond elongation of 0.012 Å upon the formation of the inclusion complex VFB:β-CD-I with the unchanged length for other bonds. Likewise for VFB:β-CD-II, an N2-H2′ bond elongation of 0.010 Å was calculated. Interestingly, such notable elongations can be attributed to strong noncovalent interactions with the host molecule. It is worth noting N1-H1′ bond is associated through HB with the oxygen atoms of the hydroxyl groups at the wide rim of the β-CD with a HB length of 1.968 and 2.105 Å for VFB:β-CD-I and VFB:β-CD-II, respectively; see below for more information. The corresponding oxygen atom of the host molecule that is involved in HB is labeled as displayed in Fig. 4.

Furthermore, another key structural change that the guest molecule exhibit upon a host-guest inclusion complexation is undergoing an induced twisted molecular conformational changes. As illustrated in Fig. 2, VFB structure bears the rings marked as A and B that are twisted out of plane with a twisting dihedral angle (α) of 140°. However, upon the formation of the complex VFB:β-CD-I, VFB as a guest molecule exhibited a substantial decrease in α rotation with a calculated value of 97° compared with a value of 140° for the uncomplexed VFB molecule. Nevertheless, it is worth noting that VFB in complexes VFB:β-CD-II, VFB:CB7-I, and VFB:CB7-II exhibited a negligible change of ± 2° in the values of α. Importantly, it can be anticipated that such substantial reduction in the coplanarity of VFB can induce a discontinuation in the charge delocalization within units A and B and consequently altering the corresponding physicochemical properties of the drug.

One the other hand, it is noteworthy mentioning that obtaining DFT-based optimized geometries of all potential inclusion complexes does not necessarily mean that they all have the same probability to be formed in solution. Thus, the key standard thermodynamic quantities for each complexation reaction were calculated at the same level of theory; this includes the changes in Gibbs free energy (ΔG°), enthalpies (ΔH°), and entropy (ΔS°). The corresponding thermodynamic quantity was calculated per the optimized geometries of all species before and after complexation. For example, eq. 2 illustrates the general formula used to calculate the ΔG° of inclusion complexation:

$$\Delta G = G^{\circ}_{complex} - - (G^{\circ}_{VFB} + G^{\circ}_{Host}) \quad (1)$$

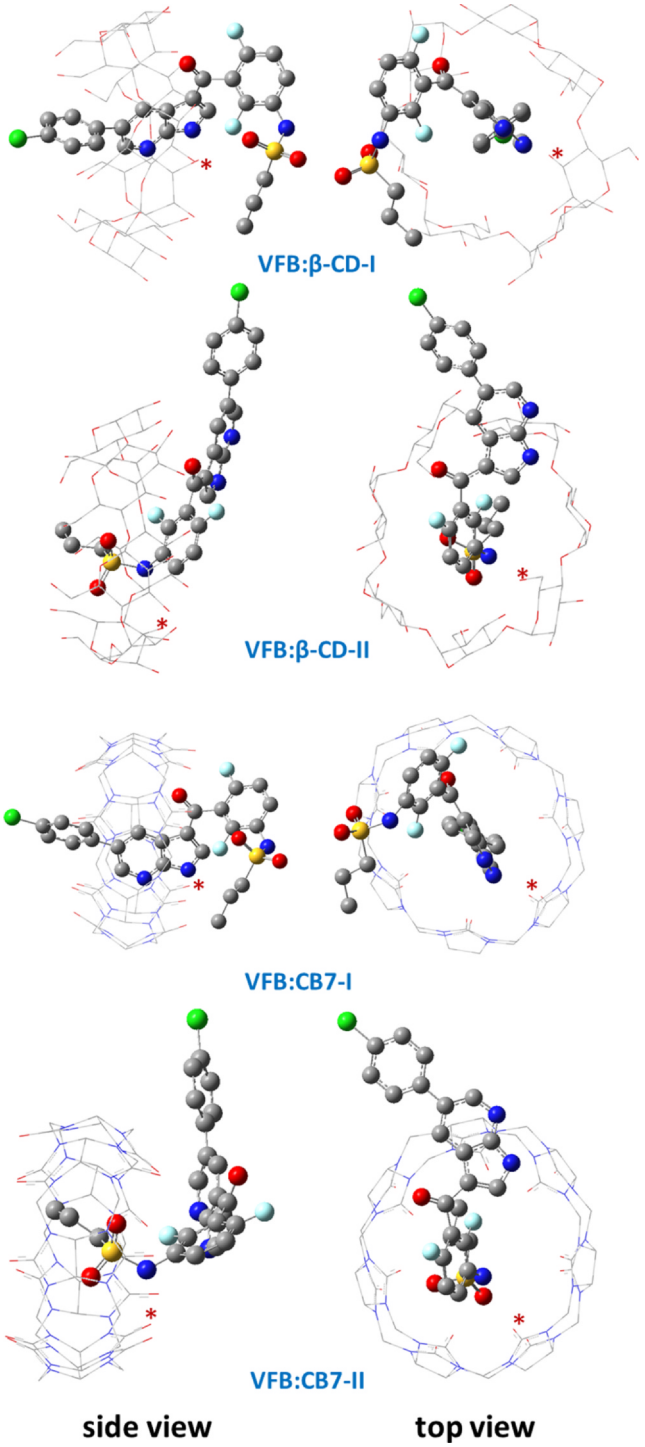

Fig. 4. Optimized geometries of VFB:β-CD and VFB:CB7 and 1:1 host-guest supramolecular assemblies; DFT/ωb97xd(6-31 g(d))/IEFPCM (water); (*) oxygen atom of the host molecule involved in HB; hydrogen atoms were omitted for clarity.

where $G^{\circ}_{complex}$, $G^{\circ}_{VFB,}$ and G°_{Host} are the thermal free energies of the molecular 1:1 host-guest supramolecular assemblies with β-CD and CB7, free (uncomplexed) drug molecule, and free host molecule, respectively. Calculated thermodynamics quantities are compiled in Table 2.

According to the calculated ΔG°, one can notice that the formation of all examined inclusion complexes is a spontaneous process. This is expectedly well in line with the nature of the nanocavities of β-CD and CB7 as well as the VFB molecule in terms of matching hydrophobicity and stabilization factor of HB at the rims of the nanocavities of the host molecules. Concerning the role of the phase of the medium, it is worth noting that there is a substantial difference in the thermodynamic quantities obtained in the gas phase (vacuum) compared to implicit aqueous solutions indicative of the significant effect of solvation on the supramolecular host-guest interactions of VFB with β-CD and CB7. For example, the formation of VFB:β-CD-I is associated with ΔG° of −28.0 and −15.3 kcal/mol in the gas and implicit aqueous phases, respectively. Also, one can notice that the DFT calculations revealed an insignificant difference upon employing β-CD and CB7 as a host in the gas phase. However, a substantial difference is observed for the role of the host in implicit aqueous phase as revealed by the DFT calculations, where ΔG° values of −15.3 and −6.2 kcal/mol were calculated for the formation of VFB:β-CD-I and VFB:CB7-I complexes, respectively. These DFT results suggest substantial favoritism for VFB to form supramolecular inclusion complexes with β-CD compared with CB7.

Furthermore, concerning the configuration of inclusion complexation, i.e. chlorobenzene versus sulfonamide inclusions, although both configurations yielded the same ΔG° values of −15.3 kcal/ mol for VFB:β-CD complexes, yet other thermodynamic quantities, namely ΔH° and ΔS° indicate a notable difference. For example, the formation of VFB:β-CD-II is favored to be formed versus VFB:β-CD-I in terms of ΔH°, yet such favoritism is notably reduced with respect to the retardation effect of ΔS°. Hence, such opposing favoritisms of ΔH° and ΔS° is balanced to afford equal favoritism in terms of ΔG°. Nevertheless, considering the relatively different hydrophobicity that is exhibited by the chlorobenzene and sulfonamide units, it can be suggested that the hydrophobicity of the guest molecule is not the key factor for the formation of the complexes. Indeed, one can anticipate an overrule contribution of another noncovalent intermolecular interaction, namely HB. Such observation is well in line with the structural changes calculated for VFB upon the formation of the complexes as summarized in Table 1. See below for further information concerning the contribution of HB.

Simulated UV–Vis absorption spectra. In order to shed more light on the effect of supramolecular inclusion complexation on the molecular properties of VFB, it is necessary to investigate the nature molecular orbitals (MOs) of VFB before and after complexation; this includes their

Table 1
Key structural parameters of the examined species.[a]

Species	Bond Length (Å)				Torsion Angle α (°)
	N1-H1′	N2-H2′	C3-F3′	C4-F4′	C5-C6-C7-C8
VFB	1.010	1.015	1.342	1.340	140
VFB:β-CD-I	1.022	1.015	1.342	1.341	97
VFB:β-CD-II	1.010	1.025	1.344	1.338	139
VFB:CB7-I	1.016	1.015	1.334	1.331	138
VFB:CB7-II	1.019	1.027	1.331	1.340	142

[a] See Fig. 2 for atom numbering.

Table 2
Thermodynamic quantities of VFB host-guest inclusion complexation with β-CD and CB7.

Complex	Thermodynamic Quantity[a]					
	Vacuum			Water		
	ΔG°	ΔH°	ΔS°	ΔG°	ΔH°	ΔS°
VFB:β-CD-I	−28.0	−45.3	−57.9	−15.3	−34.1	−63.1
VFB:β-CD-II	−29.5	−49.2	−66.0	−15.3	−36.8	−72.1
VFB:CB7-I	−27.4	−50.2	−76.7	−6.2	−29.1	−76.8
VFB:CB7-II	−30.1	−55.4	−84.7	−9.9	−34.2	−81.5

[a] ΔG and ΔH in kcal/mol, ΔS in cal/mol-K; Temperature = 298 K.

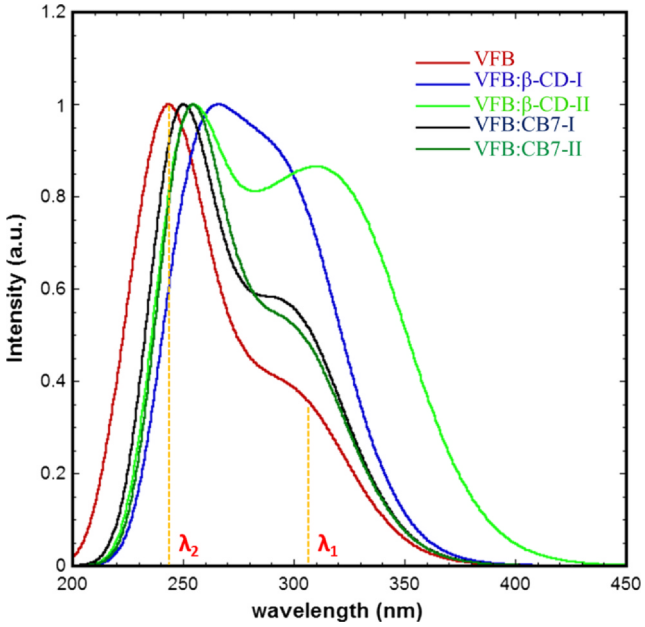

Fig. 5. Normalized simulated UV–Vis absorption spectra of VFB and 1:1 host-guest supramolecular assemblies with β-CD and CB7.

energy as well as localization/delocalization pattern. This is in fact crucial as such analyses can provide insights concerning the reactivity of the molecule and correspondingly potential photostability. To this end, simulated UV–Vis absorption spectra of substances of interest can be utilized to perform the desired MOs analysis. Fig. 5 displays the normalized simulated UV–Vis absorption spectra of all examined species in implicit aqueous solutions obtained via employing the TD-DFT/IEFPCM method.

One can notice from Fig. 5 that the absorption spectrum of free VFB molecules exhibits absorption bands centered at wavelengths (λ) of ~307 and 247 nm that are ascribed as λ_1 and λ_2, respectively. These results are in good agreement with the reported experimental results of the absorption spectrum of VFB in solution [51,52]. Also, the simulated spectra of free β-CD and CB7 did not exhibit any band in the UV–Vis range indicative of no overlapping between the calculated spectra. On the other hand, it is noteworthy mentioning that most of the phototoxicity of photosensitizing drugs is induced by exposure to sunlight of a wavelength in the range of 290–700 nm, which particularly corresponds to the sunlight that can reach the earth. As such, we focus our analysis herein on the λ_1 band in terms of shape and position within that range. Examining Fig. 5, it can be noticed that complexation with β-CD can induce a substantial effect on the shape and position of the spectrum of VFB indicative of strong interaction and consequently significant impact on the corresponding MOs. Indeed, such substantial impact on the absorption spectrum of VFB is well in line with the thermodynamic and structural analyses discussed above.

Furthermore, the most notable change concerning the shape of the absorption spectrum of VFB is observed for the complex of VFB: β-CD-I. It can be suggested that such changes in the shape of the spectrum can be attributed to the conformational changes in the structure of VFB upon complexation with β-CD-I to form the 1:1 host-guest supramolecular assembly with β-CD VFB: β-CD-I. Hence, such conformational changes might cause a rearrangement in the MOs that are responsible for the corresponding electric transitions of particular absorption bands as well as altering the probability of such transition; see below for further information. On the other hand, although the shape of the spectrum of VFB was not significantly influenced by complexation with CB-7, yet one can notice that the relative intensity I_R ($I_R = I(\lambda_1)/I(\lambda_2)$) has increased. Compared with free VFB, the I_R exhibited a change by approximately 0.55, 0.51, 0.22, and 0.15 for complexes VFB:β-CD-I, VFB:β-CD-II, VFB:CB7-I, and VFB:CB7-II, respectively.

Frontier Molecular Orbitals. In principle, the spectral bands in the absorption spectrum of a molecule correspond to particular electronic transitions between specific MOs upon being exposed to light. Hence, the induced changes in the absorption spectrum are indicative of changes in the MOs in terms of nature and/or energy. The frontier MOs of all examined species are simulated at the same level of geometry optimization. Fig. 6 displays the key MOs of the examined species, namely the HOMO and LUMO. The DFT calculation revealed that the absorption band of λ_1 corresponds to HOMO → LUMO electronic transition, which indeed indicates a nature of $\pi \rightarrow \pi^*$ transition. It is worth noting that the HOMO of VFB is extended over the conjugated part of the molecule comprising mainly the chlorobenzene and pyridine-pyrrole infused rings, whereas the LUMO is extended over mainly

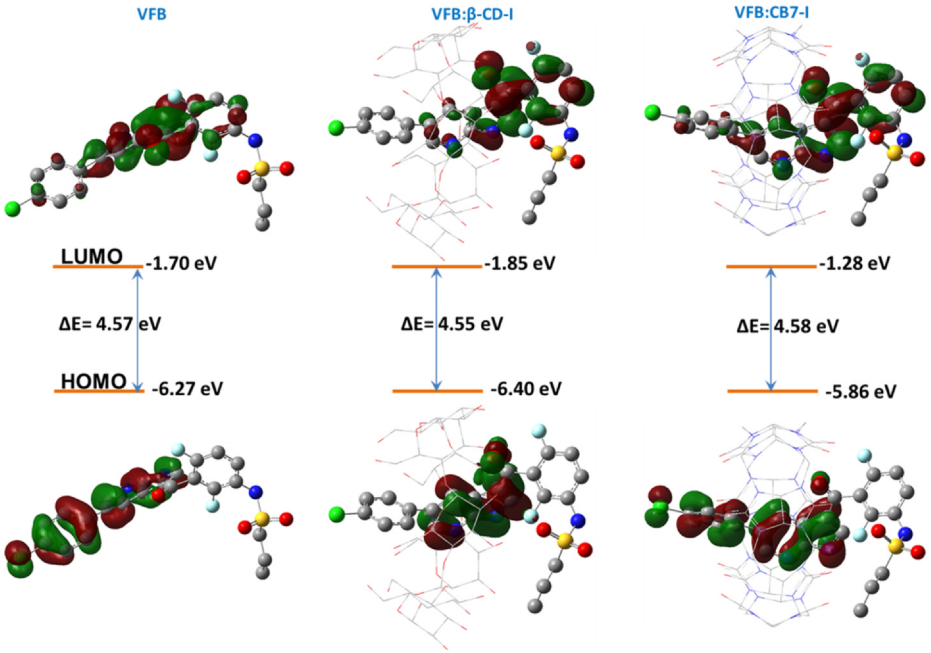

Fig. 6. The frontier MOs (HOMO-LUMO) of VFB and 1:1 host-guest supramolecular assemblies with β-CD and CB7.

the pyridine-pyrrole infused rings. An energy gap ($\Delta E = E_{LUMO}$-E_{HOMO}) of 4.57 eV was calculated for VFB. Interestingly, the formation of VFB:β-CD-I induced a substantial change in the nature of the HOMO of VFB with no change observed for the LUMO, whereas the formation of VFB:CB7-I has no effect on the nature of both MOs. Yet, it is worth noting that ΔE for both complexes has been slightly affected, where values of 4.55 and 4.58 eV were calculated for VFB:β-CD-I and VFB:CB7-I complexes, respectively. However, the formation of VFB:β-CD-II has no effect on the nature of both HOMO and LUMO of VFB. It can be noted that the delocalization HOMO of VFB has been reduced to be extended over only the pyridine-pyrrole infused rings.

Extending the MOs analysis to cover other orbitals (data not shown), the obtained results revealed that the HOMO of VFB has become HOMO-3 in VFB:β-CD-I indicative of the role of complexation in inducing MOs' rearrangement to bear out the new molecular environment inside the nanocavities. Indeed, such changes in nature and energies of the MOs of VFB upon the formation of the inclusion complexes are well in line with the results obtained from the absorption spectrum. These results suggest that although the ΔE of VFB:β-CD-I has been reduced indicating a red-shift in the spectral properties, yet the original HOMO of VFB has been stabilized as it has been located as HOMO-3 after complexation. It can be suggested that such spectral shift might be attributed to the conformational changes that the guest molecule VFB exhibits upon the formation of the 1:1 host-guest supramolecular assemblies with β-CD. However, comparing the absorption spectrum of VFB:β-CD-I with VFB:β-CD-II, it is apparent that VFB:β-CD-I exhibits a blue-shift in λ_1 compared to VFB:β-CD-II. It can be suggested that such relative blue-shift is attributed to the conformational changes in VFB upon the formation of VFB:β-CD-I as discussed above, which can cause a reduction in the extent of conjugation and consequently inducing a blue-shift in the corresponding absorption band. Importantly, it can be suggested that the photochemical behavior originated from the HOMO of VFB is notably affected by supramolecular interaction with β-CD and consequently reduction in the drug phototoxicity might be anticipated.

NBO analyses. In view of the results discussed above, the noncovalent interactions associated with the formation of the inclusion complexes of VFB with β-CD and CB7 were further assessed employing the NBO method. In this approach, the noncovalent interactions are visualized in terms of donor → acceptor interactions between two MOs, which in turn corresponds to a charge transfer from a donor MO to an acceptor MO. Henceforth, such interaction is considered as a stabilizing factor that promotes the formation of the species of interest, namely the inclusion complexes. Such interactions are quantitatively assessed employing the second-order perturbation energy of interaction (E(2)). To this end, we focused herein on the key noncovalent interactions that exhibit notable stabilizing energy, namely the HBs; see Table 3. As can be noted, the VFB:β-CD complexes are stabilized by two cooperative HBs, namely $lp(O)_{\beta\text{-CD}} \rightarrow \sigma^*(N{-}H)_{VFB}$ and $lp(O)_{VFB} \rightarrow \sigma^*(O{-}H)_{\beta\text{-CD}}$. The calculations revealed E(2) values of 11.5 and 3.9 kcal/mol, respectively. For complex VFB:β-CD-I and 4.9 and 7.3 kcal/mol, respectively, for complex VFB:β-CD-II. Furthermore, the average length of these HBs (d_{HB}) are centered on a value of approximately 2.000 Å indicative of strong HB. Comparing these results with VFB:CB7 complexes, one can notice that CB7 can exhibit only one type of interaction, namely $lp(O)_{CB7} \rightarrow \sigma^*(N{-}H)_{VFB}$, indicative of reduced stabilizing interaction compared to VFB:β-CD complexes. Fig. 7 illustrates a graphical comparison between VFB:β-CD-I versus VFB:CB7-I. In addition, it is worth noting that the HB occurs at the rims of both host molecules. Interestingly, these NBO results are well in line with the thermodynamic results presented above in terms of energy of interaction between the VFB as a guest molecule and β-CD and CB7 as host molecules.

Table 3
NBO electronic transitions of the intermolecular HB of VFB host-guest inclusion complexation with β-CD and CB7 and the corresponding stabilization energies (E(2)).

Complex	Transition (donor → acceptor)	E(2) kcal/mol	d_{HB} Å
VFB:β-CD (I)	$lp(O)_{\beta\text{-CD}} \rightarrow \sigma^*(N{-}H)_{VFB}$	11.5	1.968
	$lp(O)_{VFB} \rightarrow \sigma^*(O{-}H)_{\beta\text{-CD}}$	3.9	2.059
VFB:β-CD (II)	$lp(O)_{\beta\text{-CD}} \rightarrow \sigma^*(N{-}H)_{VFB}$	4.9	2.105
	$lp(O)_{VFB} \rightarrow \sigma^*(O{-}H)_{\beta\text{-CD}}$	7.3	1.842
VFB:CB7 (I)	$lp(O)_{CB7} \rightarrow \sigma^*(N{-}H)_{VFB}$	5.1	1.989
VFB:CB7 (II)	$lp(O)_{CB7} \rightarrow \sigma^*(N{-}H)_{VFB}$	8.7	1.842

Furthermore, it is noteworthy to mention that both host and guest molecules may undergo conformational changes upon the formation of the molecular host-guest supramolecular assemblies, and hence it is essential to examine the potentiality of such conformational changes in terms of energy and geometrical aspects of the corresponding supramolecular assemblies. In light of the results obtained for the energy of interaction and stabilization factors, the stability of the studied host-guest supramolecular assemblies was further examined employing the ADMP molecular dynamics approach. Fig. 8 illustrates the changes in the total energy (ΔE, kcal/mol)) of the optimized geometries of the inclusion complexes as well as changes in the length of the key HB (Δd_{HB}).

As can be noted, the host-guest supramolecular assemblies of VFB with β-CD and CB7 exhibit a ΔE of ± 0.02 kcal/mol indicative of substantial dynamic stability over the tested time frame. Furthermore, the key HBs exhibited a Δd_{HB} of only ± 0.06 Å indicative of stable intermolecular HB between VFB as a guest molecule and β-CD and CB7 as host molecules. These results suggest that both molecules of the host and guest species can exhibit a negligible conformational upon the formation of 1:1 host-guest supramolecular assemblies.

Moreover, further conformational analyses was conducted concerning other potential conformations of the examined complexes. The DFT-optimized geometry for each complex is considered as a reference input geometry (designated as R in Fig. 9). The guest molecule of VFB was systematically displaced inward and outward inside the host's cavity with a displacement of −2 and +3 Å, respectively, with an increment of 1 Å unless otherwise noted. It is noteworthy mentioning that due to the high computational cost associated with employing the DFT method for such conformational analysis, the method of semi-empirical (PM7) was employed as proof of principle. After each displacement of 1 Å, the geometry was optimized employing the semi-empirical (PM7) without any constrains. The DFT-optimized geometry was re-optimized using the same semi-empirical (PM7) method for comparison.

Fig. 9 illustrates the variation in ΔE as a function of displacement inside the host's cavity for all examined complexes relative to the reference geometry of the corresponding complex. Examples of the input geometry and the corresponding optimized geometry after selected displacements for the complex VFB:β-CD-I are displayed in Fig. 9. It is worth noting that the optimized geometries of all complexes after displacement exhibit a reasonable pattern indicative of alike behavior of complexation. For example, for complex VFB:β-CD-I, inward displacements of −1 and −2 Å induced a decrease in the stability of the complex by 0.2 and 1.5 kcal/mol, respectively, which in turn can be attributed to increased electronic repulsion. On the other hand, outward displacement of +3 Å induced a decrease in the total energy of the complex by 2.3 kcal/mol. It can be suggested that such a decrease in energy of the complex is attributed to the long distance induced by the displacement between the host and guest molecules that can consequently lead to weaker noncovalent bondings. Interestingly, these findings are well in line with the DFT-optimized geometry concerning the significance of HB as a key noncovalent bonding that has a major contribution in stabilizing the formed host-guest supramolecular assemblies.

4. Concluding remarks

The findings of the present work demonstrate the potential of VFB

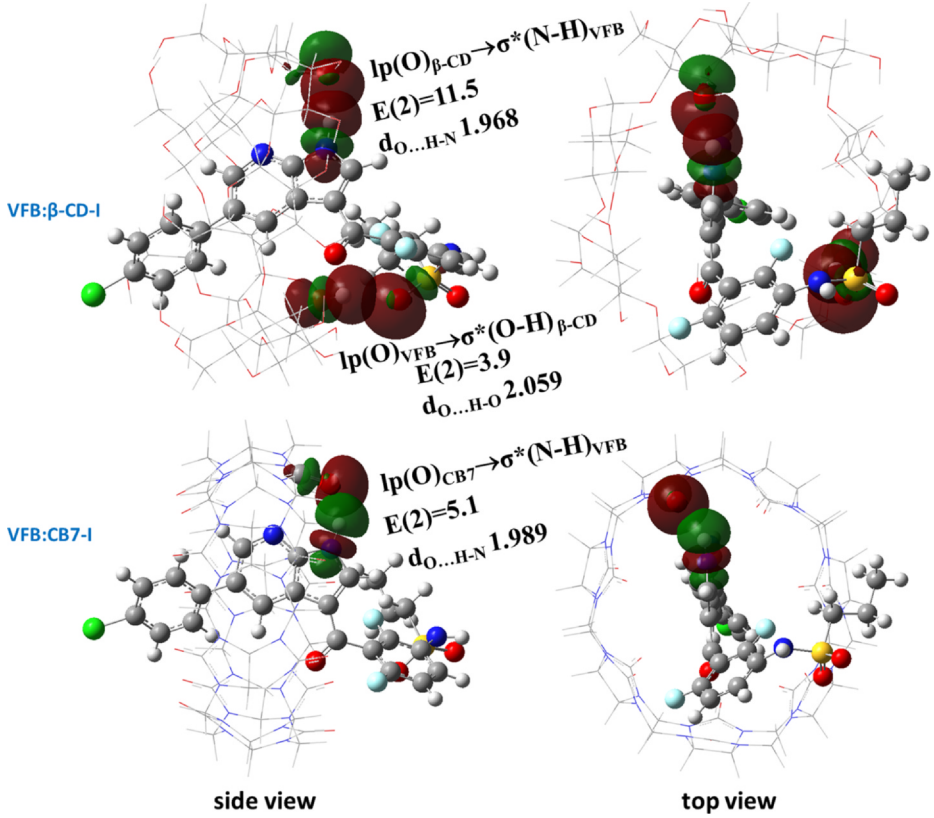

Fig. 7. Superpositions of the NBOs involved in the intermolecular HB of VFB:β-CD(I) and VFB:CB7 (I) assemblies.

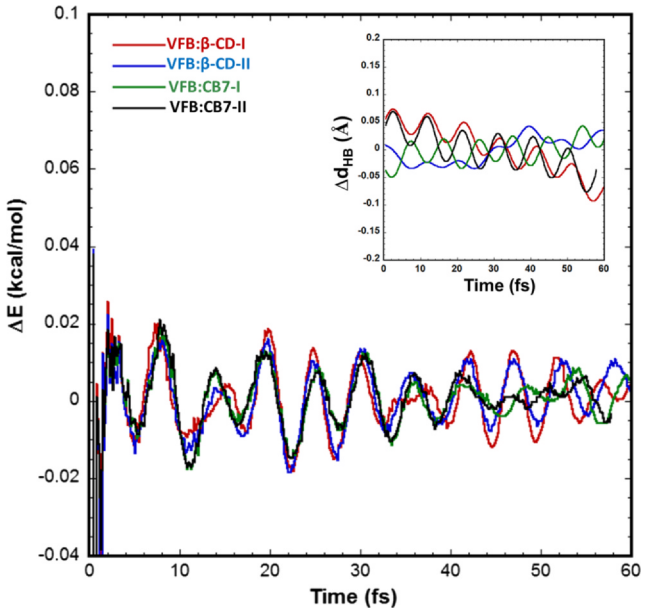

Fig. 8. The change in total energy (ΔE_{total},kcal/mol) of the optimized geometry of VFB inclusion complexes with β-CD andCB7 under dynamic simulations using the ADMP method (step size = 0.2 fs); inset: the change in the length ($\Delta d_{HB,}$ Å) of key HBs of all examined host-guest supramolecular assemblies.

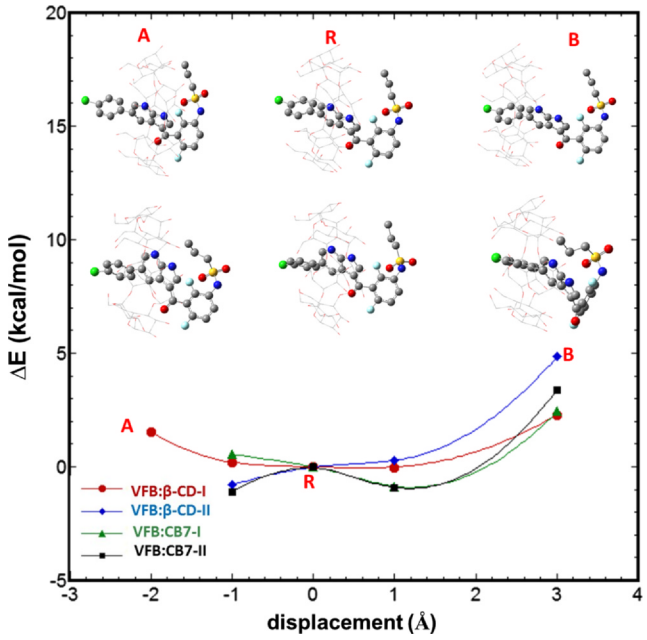

Fig. 9. The relative change in energy (ΔE, kcal/mol) of the optimized geometry of VFB inclusion complexes with β-CD andCB7 with conformations; inset: the input geometry of VFB:β-CD-I with selected displacements (up) and the corresponding semi-empirical (PM7) optimized geometry (down).

to form supramolecular host-guest inclusion complexes in aqueous solutions with two types of host molecules, namely β-CD and CB7. The DFT results suggest that these complexes are stabilized by strong intermolecular HBs between the host and guest molecules. The effect of such complexation on the physicochemical properties of VFB was demonstrated per the notable structural changes exhibited by VFB after complexation. The cooperative HBs exhibited by VFB:β-CD complexes and the associated thermodynamic quantities are indicative of the favoritism of VFB to form supramolecular host-guest complexes with β-CD compared to CB-7. The TD-DFT results demonstrated that such complexation can induce a substantial change in the spectral properties of VFB originated from stabilizing the ground state of VFB and the

corresponding electronic transitions. The NBO results revealed the particular MOs involved in the key HBs and the stabilizing energy of interaction, which are interestingly well in line with the thermodynamic and TD-DFT results. The ADMP molecular dynamics demonstrated the high stability of the complexes with negligible changes in the total energy and length of key HBs. The results reported herein suggest that the host-guest supramolecular interaction can be potentially utilized in future efforts toward reducing side effects of phototoxicity of the first-line anticancer drug VFB.

Declaration of Competing Interest

The authors declare that they have no known competing financial interests or personal relationships that could have appeared to influence the work reported in this paper.

Acknowledgments

This work was supported by the Qatar University, Qatar, (QUCD-CAS-2020-1). Major aspects of the calculations were performed using the supercomputing facility at Texas A&M University at Qatar.

References

[1] S. Murugesan, T. Scheibel, Copolymer/clay nanocomposites for biomedical applications, Adv. Funct. Mater. 30 (2020) 1908101, https://doi.org/10.1002/adfm.201908101.
[2] G. Chen, I. Roy, C. Yang, P.N. Prasad, Nanochemistry and nanomedicine for nanoparticle-based diagnostics and therapy, Chem. Rev. 116 (2016) 2826–2885, https://doi.org/10.1021/acs.chemrev.5b00148.
[3] E.C. Dreaden, A.M. Alkilany, X. Huang, C.J. Murphy, M.A. El-Sayed, The golden age: gold nanoparticles for biomedicine, Chem. Soc. Rev. 41 (2012) 2740–2779, https://doi.org/10.1039/C1CS15237H.
[4] Z. Qiu, D. Tang, Nanostructure-based photoelectrochemical sensing platforms for biomedical applications, J. Mater. Chem. B. 8 (2020) 2541–2561, https://doi.org/10.1039/C9TB02844G.
[5] R.R. Arvizo, S. Bhattacharyya, R.A. Kudgus, K. Giri, R. Bhattacharya, P. Mukherjee, Intrinsic therapeutic applications of noble metal nanoparticles: past, present and future, Chem. Soc. Rev. 41 (2012) 2943, https://doi.org/10.1039/c2cs15355f.
[6] T. Sun, Y.S. Zhang, B. Pang, D.C. Hyun, M. Yang, Y. Xia, Engineered nanoparticles for drug delivery in cancer therapy, Angew. Chem. Int. Ed. (2014) n/a-n/a, https://doi.org/10.1002/anie.201403036.
[7] E.-K. Lim, T. Kim, S. Paik, S. Haam, Y.-M. Huh, K. Lee, Nanomaterials for theranostics: recent advances and future challenges, Chem. Rev. 115 (2015) 327–394, https://doi.org/10.1021/cr300213b.
[8] S. Mura, J. Nicolas, P. Couvreur, Stimuli-responsive nanocarriers for drug delivery, Nat. Mater. 12 (2013) 991–1003, https://doi.org/10.1038/nmat3776.
[9] L. Vigderman, E.R. Zubarev, Therapeutic platforms based on gold nanoparticles and their covalent conjugates with drug molecules, Adv. Drug Deliv. Rev. 65 (2013) 663–676, https://doi.org/10.1016/j.addr.2012.05.004.
[10] S.S. Said, S. Campbell, T. Hoare, Externally addressable smart drug delivery vehicles: current technologies and future directions, Chem. Mater. 31 (2019) 4971–4989, https://doi.org/10.1021/acs.chemmater.9b01798.
[11] K. Sztandera, M. Gorzkiewicz, B. Klajnert-Maculewicz, Gold nanoparticles in cancer treatment, Mol. Pharm. 16 (2019) 1–23, https://doi.org/10.1021/acs.molpharmaceut.8b00810.
[12] M. Wu, X. Lin, X. Tan, J. Li, Z. Wei, D. Zhang, Y. Zheng, A. Zheng, B. Zhao, Y. Zeng, X. Liu, J. Liu, Photoresponsive nanovehicle for two independent wavelength light-triggered sequential release of P-gp shRNA and doxorubicin to optimize and enhance synergistic therapy of multidrug-resistant cancer, ACS Appl. Mater. Interfaces 10 (2018) 19416–19427, https://doi.org/10.1021/acsami.8b03823.
[13] X. Ma, Y. Zhao, Biomedical applications of supramolecular systems based on host-guest interactions, Chem. Rev. 115 (2015) 7794–7839, https://doi.org/10.1021/cr500392w.
[14] R. Mejia-Ariza, L. Graña-Suárez, W. Verboom, J. Huskens, Cyclodextrin-based supramolecular nanoparticles for biomedical applications, J. Mater. Chem. B. 5 (2017) 36–52, https://doi.org/10.1039/C6TB02776H.
[15] L. Isaacs, Stimuli responsive systems constructed using cucurbit[n]uril-type molecular containers, Acc. Chem. Res. 47 (2014) 2052–2062, https://doi.org/10.1021/ar500075g.
[16] Q.-D. Hu, G.-P. Tang, P.K. Chu, Cyclodextrin-based host-guest supramolecular nanoparticles for delivery: from design to applications, Acc. Chem. Res. 47 (2014) 2017–2025, https://doi.org/10.1021/ar500055s.
[17] H.J. Schneider, Binding mechanisms in supramolecular complexes, Angew. Chemie - Int. Ed. (2009), https://doi.org/10.1002/anie.200802947.
[18] K. Uekama, F. Hirayama, T. Irie, Cyclodextrin drug carrier systems, Chem. Rev. (1998), https://doi.org/10.1021/cr970025p.
[19] A. Harada, Cyclodextrin-Based Molecular Machines †, Acc. Chem. Res. 34 (2001) 456–464, https://doi.org/10.1021/ar000174l.
[20] G. Crini, Review: a history of cyclodextrins, Chem. Rev. 114 (2014) 10940–10975, https://doi.org/10.1021/cr500081p.
[21] S.J. Barrow, S. Kasera, M.J. Rowland, J. del Barrio, O.A. Scherman, Cucurbituril-Based Molecular Recognition, Chem. Rev. 115 (2015) 12320–12406, https://doi.org/10.1021/acs.chemrev.5b00341.
[22] J. Lagona, P. Mukhopadhyay, S. Chakrabarti, L. Isaacs, The Cucurbit[n]uril Family, Angew. Chemie Int. Ed. 44 (2005) 4844–4870, https://doi.org/10.1002/anie.200460675.
[23] K. Müller-Dethlefs, P. Hobza, Noncovalent Interactions: A Challenge for Experiment and Theory, Chem. Rev. 100 (2000) 143–168, https://doi.org/10.1021/cr9900331.
[24] D. Umadevi, S. Panigrahi, G.N. Sastry, Noncovalent Interaction of Carbon Nanostructures, Acc. Chem. Res. 47 (2014) 2574–2581, https://doi.org/10.1021/ar500168b.
[25] A.D. Bani-Yaseen, A.S. Al-Jaber, H.M. Ali, Probing the Solute-Solvent Interaction of an Azo-Bonded Prodrug in Neat and Binary Media: Combined Experimental and Computational Study, Sci. Rep. 9 (2019) 3023, https://doi.org/10.1038/s41598-019-39028-1.
[26] M. Shkoor, H. Mehanna, A. Shabana, T. Farhat, A.D. Bani-Yaseen, Experimental and DFT/TD-DFT computational investigations of the solvent effect on the spectral properties of nitro substituted pyridino[3,4-c]coumarins, J. Mol. Liq. (2020), https://doi.org/10.1016/j.molliq.2020.113509.
[27] H. Wang, H. Liu, F.-Q. Bai, S. Qu, X. Jia, X. Ran, F. Chen, B. Bai, C. Zhao, Z. Liu, H.-X. Zhang, M. Li, Theoretical and experimental study on intramolecular charge-transfer in symmetric bi-1,3,4-oxadiazole derivatives, J. Photochem. Photobiol. A Chem. 312 (2015) 20–27, https://doi.org/10.1016/j.jphotochem.2015.07.006.
[28] A.D. Bani-Yaseen, Computational insights into the photocyclization of diclofenac in solution: Effects of halogen and hydrogen bonding, Phys. Chem. Chem. Phys. 18 (2016) 21322–21330, https://doi.org/10.1039/c6cp03671f.
[29] P. Hobza, K. Müller-Dethlefs, Non-covalent interactions: Theory and experiment, RSC Theor. Comput. Chem. Ser. (2009).
[30] A.D. Bani-Yaseen, M. Al-Balawi, The solvatochromic, spectral, and geometrical properties of nifenazone: a DFT/TD-DFT and experimental study, Phys. Chem. Chem. Phys. 16 (2014) 15519–15526, https://doi.org/10.1039/C4CP01679C.
[31] A.D. Bani-Yaseen, F. Hammad, B.S. Ghanem, E.G. Mohammad, On the Photophysicochemical Properties of Selected Fluoroquinolones: Solvatochromic and Fluorescence Spectroscopy Study, J. Fluoresc. 23 (2013) 93–101, https://doi.org/10.1007/s10895-012-1120-7.
[32] A.D. Bani-Yaseen, Solvatochromic and Fluorescence Behavior of Sulfisoxazole, J. Fluoresc. 21 (2011) 1061–1067, https://doi.org/10.1007/s10895-010-0778-y.
[33] A.S. Al-Jaber, A.D. Bani-Yaseen, On the encapsulation of Olsalazine by β-cyclodextrin: A DFT-based computational and spectroscopic investigations, Spectrochim, Acta Part A Mol. Biomol. Spectrosc. 214 (2019) 531–536, https://doi.org/10.1016/j.saa.2019.02.030.
[34] A.D. Bani-Yaseen, Computational molecular perspectives on the interaction of propranolol with β-cyclodextrin in solution: Towards the drug-receptor mechanism of interaction, J. Mol. Liq. 227 (2017) 280–290, https://doi.org/10.1016/J.MOLLIQ.2016.12.023.
[35] A.D. Bani-Yaseen, Synchronous spectrofluorimetric study of the supramolecular host-guest interaction of β-cyclodextrin with propranolol: A comparative study, Spectrochim. Acta. A. Mol. Biomol. Spectrosc. 148 (2015) 93–98, https://doi.org/10.1016/j.saa.2015.03.128.
[36] R. Kreutz, E.A.H. Algharably, A. Douros, Reviewing the effects of thiazide and thiazide-like diuretics as photosensitizing drugs on the risk of skin cancer, J. Hypertens. 37 (2019) 1950–1958, https://doi.org/10.1097/HJH.0000000000002136.
[37] W. Ben Kim, A.J. Shelley, K. Novice, J. Joo, H.W. Lim, S.J. Glassman, Drug-induced phototoxicity: A systematic review, J. Am. Acad. Dermatol. 79 (2018) 1069–1075, https://doi.org/10.1016/j.jaad.2018.06.061.
[38] A.M. Drucker, C.F. Rosen, Drug-Induced Photosensitivity, Drug Saf. 34 (2011) 821–837, https://doi.org/10.2165/11592780-000000000-00000.
[39] K. Kim, H. Park, K.-M. Lim, Phototoxicity: Its Mechanism and Animal Alternative Test Methods, Toxicol. Res. 31 (2015) 97–104, https://doi.org/10.5487/TR.2015.31.2.097.
[40] K.T. Flaherty, U. Yasothan, P. Kirkpatrick, Vemurafenib, Nat. Rev. Drug Discov. (2011), https://doi.org/10.1038/nrd3579.
[41] P.B. Chapman, A. Hauschild, C. Robert, J.B. Haanen, P. Ascierto, J. Larkin, R. Dummer, C. Garbe, A. Testori, M. Maio, D. Hogg, P. Lorigan, C. Lebbe, T. Jouary, D. Schadendorf, A. Ribas, S.J. O'Day, J.A. Sosman, J.M. Kirkwood, A.M.M. Eggermont, B. Dreno, K. Nolop, J. Li, B. Nelson, J. Hou, R.J. Lee, K.T. Flaherty, G.A. McArthur, Improved Survival with Vemurafenib in Melanoma with BRAF V600E Mutation, N. Engl. J. Med. 364 (2011) 2507–2516, https://doi.org/10.1056/NEJMoa1103782.
[42] G. Bollag, J. Tsai, J. Zhang, C. Zhang, P. Ibrahim, K. Nolop, P. Hirth, Vemurafenib: the first drug approved for BRAF-mutant cancer, Nat. Rev. Drug Discov. 11 (2012) 873–886, https://doi.org/10.1038/nrd3847.
[43] M. Das Thakur, F. Salangsang, A.S. Landman, W.R. Sellers, N.K. Pryer, M.P. Levesque, R. Dummer, M. McMahon, D.D. Stuart, Modelling vemurafenib resistance in melanoma reveals a strategy to forestall drug resistance, Nature 494 (2013) 251–255, https://doi.org/10.1038/nature11814.
[44] P.A. Ascierto, G.A. McArthur, B. Dréno, V. Atkinson, G. Liszkay, A.M. Di Giacomo, M. Mandalà, L. Demidov, D. Stroyakovskiy, L. Thomas, L. de la Cruz-Merino, C. Dutriaux, C. Garbe, Y. Yan, M. Wongchenko, I. Chang, J.J. Hsu, D.O. Koralek, I. Rooney, A. Ribas, J. Larkin, Cobimetinib combined with vemurafenib in advanced BRAFV600-mutant melanoma (coBRIM): updated efficacy results from a randomised, double-blind, phase 3 trial, Lancet Oncol. 17 (2016) 1248–1260, https://doi.

org/10.1016/S1470-2045(16)30122-X.
[45] P. Gelot, H. Dutartre, A. Khammari, A. Boisrobert, C. Schmitt, J.-C. Deybach, J.-M. Nguyen, S. Seité, B. Dréno, Vemurafenib: an unusual UVA-induced photosensitivity, Exp. Dermatol. 22 (2013) 297–298, https://doi.org/10.1111/exd.12119.
[46] L. Boussemart, C. Boivin, J. Claveau, Y.G. Tao, G. Tomasic, E. Routier, C. Mateus, E. Deutsch, C. Robert, Vemurafenib and Radiosensitization, JAMA Dermatology. 149 (2013) 855, https://doi.org/10.1001/jamadermatol.2013.4200.
[47] S.M. Boudon, U. Plappert-Helbig, A. Odermatt, D. Bauer, Characterization of Vemurafenib Phototoxicity in a Mouse Model, Toxicol. Sci. 137 (2014) 259–267, https://doi.org/10.1093/toxsci/kft237.
[48] G.E.. Frisch, M. J.; Trucks, G. W.; Schlegel, H. B.; Scuseria, V.. M. Robb, M. A.; Cheeseman, J. R.; Scalmani, G.; Barone, H. B.; Petersson, G. A.; Nakatsuji, H.; Caricato, M.; Li, X.; Hratchian, M.. P.; Izmaylov, A. F.; Bloino, J.; Zheng, G.; Sonnenberg, J. L.; Hada, M.. N. Ehara, M.; Toyota, K.; Fukuda, R.; Hasegawa, J.; Ishida, J.. T.; Honda, Y.; Kitao, O.; Nakai, H.; Vreven, T.; Montgomery, J. A., E.N.. Peralta, J. E.; Ogliaro, F.; Bearpark, M. J.; Heyd, J.; Brothers, J.. Kudin, K. N.; Staroverov, V. N.; Kobayashi, R.; Normand, S.S.. Raghavachari, K.; Rendell, A. P.; Burant, J. C.; Iyengar, J.E.. Tomasi, J.; Cossi, M.; Rega, N.; Millam, N. J.; Klene, M.; Knox, R.. Cross, J. B.; Bakken, V.; Adamo, C.; Jaramillo, J.; Gomperts, C.. Stratmann, R. E.; Yazyev, O.; Austin, A. J.; Cammi, R.; Pomelli, V.G.. Ochterski, J. W.; Martin, R. L.; Morokuma, K.; Zakrzewski, A. Voth, G. A.; Salvador, P.; Dannenberg, J. J.; Dapprich, S.; Daniels, D.J. D.; Farkas, O.; Foresman, J. B.; Ortiz, J. V.; Cioslowski, J.; Fox, Gaussian 09, Gaussian, Inc. Wallingford, CT,. (n.d.).
[49] MOPAC2016, Version: 16.076W, James J. P. Stewart, Stewart Computational Chemistry, web: HTTP://OpenMOPAC.net., (n.d.) 2016.
[50] J. Tomasi, B. Mennucci, E. Cancès, The IEF version of the PCM solvation method: an overview of a new method addressed to study molecular solutes at the QM ab initio level, J. Mol. Struct. Theochem. 464 (1999) 211–226, https://doi.org/10.1016/S0166-1280(98)00553-3.
[51] P. Morlière, F. Boscá, A.M.S. Silva, A. Teixeira, A. Galmiche, J.-C. Mazière, V. Nourry, J. Ferreira, R. Santus, P. Filipe, A molecular insight into the phototoxic reactions observed with vemurafenib, a first-line drug against metastatic melanoma, Photochem. Photobiol. Sci. 14 (2015) 2119–2127, https://doi.org/10.1039/C5PP00231A.
[52] R. Horbert, B. Pinchuk, P. Davies, D. Alessi, C. Peifer, Photoactivatable Prodrugs of Antimelanoma Agent Vemurafenib, ACS Chem. Biol. 10 (2015) 2099–2107, https://doi.org/10.1021/acschembio.5b00174.